

BINARY COPPER AND MANGANESE OXIDE NANOPARTICLES SUPPORTED OMS-2 FOR ENHANCING ACTIVITY AND STABILITY TOWARD CO-OXIDATION REACTION AT LOW TEMPERATURE

Nguyen Trung Thanh, Nguyen Thi Quynh Anh*

*Department of Environmental Engineering, An Giang University,
18 Ung Van Khiem, Long Xuyen City, An Giang Province*

*Email: ntqanh@agu.edu.vn

Received: 4 September 2018, Accepted for publication: 5 December 2018

ABSTRACT

CuO, CuMnO_x and MnO_x catalysts were anchored on the manganese oxide support with the structure of octahedral molecular sieves (OMS-2), which were synthesized using MnSO₄ and KMnO₄ as precursors by refluxing under acidic conditions or impregnation. The catalysts were then tested for CO oxidation. These catalysts and OMS-2 support were characterized by X-ray diffraction, FTIR, SEM, and H₂-TPR. For CO oxidation reaction, CuO and CuMnO_x catalysts showed extremely higher activities than that of MnO_x catalyst and OMS-2 support. The 100 % conversion of CO (T₁₀₀) for the CuO and CuMnO_x catalysts were observed at 55 °C and 65 °C, respectively. Due to the presence of Cu²⁺–O²⁻–Mn⁴⁺ ↔ Cu⁺–□–Mn³⁺ + O₂ the redox couple in the structure of these solid catalyst. Additionally, the CuMnO_x catalyst showed higher activity (~1.74 folds) and exhibited better stability than CuO catalyst in CO oxidation, due to the advanced functionality of binary oxide structure of CuMnO_x catalyst. As known, CO oxidation may follow the Mars-van-Krevelen mechanism with Cu²⁺–O²⁻–Mn⁴⁺ ↔ Cu⁺–□–Mn³⁺ + O₂ redox couple. This study shows the high application potential of CuMnO_x/OMS-2 material in treatment of CO.

Keywords: binary oxide catalyst structure; manganese oxide octahedral molecular sieves; low temperature CO oxidation, advanced CuO/OMS-2 catalyst, Mars-van-Krevelen mechanism.

Classification numbers: 2.4.2, 2.10.1, 3.4.5.

1. INTRODUCTION

The catalyst for CO oxidation has wide applications in indoor air cleaning, CO gas sensors, CO₂ lasers, and automotive exhaust treatment [1, 2]. Generally, precious-metal catalysts such as Au/TiO₂, Au/ZrO₂, Pt/SnO₂ and Pt/SiO₂ have been used for low-temperature CO oxidation [3-5]. However, due to the high cost of precious metals, more attention has recently been given to the use of base-metal catalysts, especially copper catalysts [6-8]. Among them,

Cu–Ce–O catalysts are of special interest due to their remarkable activities that are even comparable to the noble metals [9, 10]. Namely, Chen et al. found that finely dispersed CuO species were the active phase for CO oxidation [8].

Octahedral molecular sieves (OMS-2) of manganese oxides are cryptomelane-typed manganese oxides with a porous structure (0.46 nm) arising from edge sharing of 2×2 $[\text{MnO}_6]$ octahedral chains to form one-dimensional tunnel structures [11, 12]. Mn species in the OMS-2 material have mixed-valent Mn^{4+} , Mn^{3+} , and some Mn^{2+} sites. Divalent and trivalent transition metal ions incorporated into OMS-2 have been developed as promising catalysts for oxidation reactions [13], such as selective oxidation of benzyl alcohol and cyclohexane, as well as oxidation of methanol for fuel cell applications [14, 15]. Moreover, Ag-OMS-2 has been reported as an active catalyst for the CO oxidation [16]. Especially, Liu et al. found that CuO catalysts supported on OMS-2 (CuO/OMS-2) were highly active for CO oxidation at low temperature (90 % conversion of CO at 55 °C) due to the Mars-van-Krevelen mechanism with $\text{Cu}^{2+} - \text{O}^{2-} - \text{Mn}^{4+} \leftrightarrow \text{Cu}^+ - \square - \text{Mn}^{3+} + \text{O}_2$ (\square - oxygen vacancy) redox couple [17].

However, for copper oxide nanocatalyst on OMS-2 support, the efficiency of CO conversion is extremely low per a copper metal atom, because the Mars-van-Krevelen mechanism with $\text{Cu}^{2+} - \text{O}^{2-} - \text{Mn}^{4+} \leftrightarrow \text{Cu}^+ - \square - \text{Mn}^{3+} + \text{O}_2$ redox couple could be seen at the contact sites of CuO nanoparticles and OMS-2 support. Meanwhile, the less interaction of Cu-O-Mn is obtained. In the present study, the catalyst of CuO and MnO_x mixture on OMS-2 ($\text{CuMnO}_x/\text{OMS-2}$) was prepared and tested with CO oxidation reaction. For comparison, the CuO catalyst on OMS-2 support was also synthesized. It was found that the $\text{CuMnO}_x/\text{OMS-2}$ catalyst showed very high catalytic activity for CO oxidation reaction at low temperature. This study showed the prepared material is a potential catalyst for exhaust treatment with CO contamination.

2. EXPERIMENTAL SECTION

2.1. Catalyst preparation

Manganese oxide octahedral molecular sieves (OMS-2) were synthesized by a reflux method [18]. A typical synthesis was as followed: 11.33 g of $\text{MnSO}_4 \cdot \text{H}_2\text{O}$ (0.072 mol) dissolved in 120 mL of deionized water was added to a solution of 7.57 g of KMnO_4 (0.045 mol) in 38 mL of deionized water and 4 mL of concentrated HNO_3 . The mixed solution was refluxed at 100 °C for 24 h, and the product was filtered, washed, and dried at 120 °C. The dried sample was calcined at 400 °C for 4 h and denoted as OMS-2 in the text.

15 wt.% CuO/OMS-2; 15 wt.% $\text{CuMnO}_x/\text{OMS-2}$ and 15 wt.% $\text{MnO}_x/\text{OMS-2}$ catalysts were prepared by an incipient wetness method to anchor the nanoparticles of CuO, CuMnO_x and MnO_x onto the OMS-2 support. The support was immersed with a proper amount of $\text{Cu}(\text{NO}_3)_2$ and/or $\text{Mn}(\text{NO}_3)_2$ in 250 mL distilled water. The slurry was heated at 80 °C under stirring for 15 min to remove the water, followed by a calcination at 400 °C for 4 h in air [17, 19].

2.2. Samples characterizations

A wide angle X-ray diffraction (WAXRD) patterns were recorded on a D2 Phaser XRD 300 W diffractometer using Cu K_α radiation ($\lambda = 1.5406 \text{ \AA}$) with an angle step of 0.05° and a

time step of 30 s. The morphology and particle sizes of catalysts were evaluated using Transmission Electron Microscopy (TEM). Brunauer–Emmett–Teller (BET) surface area and pore size of the OMS-2 support were determined from the N₂ adsorption/desorption isotherms at 77 K (Porous Materials, BET-202A). Before the BET measurement, the support was degassed at 150 °C for 24 h to completely remove residual water from the oxide meso-/micro-pores. Accordingly, the BET data shown here are corresponding to the annealed samples. The temperature-programmed reduction (H₂-TPR, 10 vol% H₂/Ar mixture) analysis is performed on an AMI 300 chemisorption analyzer (Altamira instrument company) with a thermal conductivity detector (TCD).

2.3. Examination of metal ionic concentrations

The CuO, CuMnO_x, and MnO_x loadings on the OMS-2 support were determined by analyzing the Cu and Mn concentrations in the fresh aqueous solution of Mn(NO₃)₂ and Cu(NO₃)₂ chemicals using inductively coupled plasma-atomic emission spectrometry (ICP-AES).

2.4. Catalytic activity measurement

The CO oxidation was performed in a quartz tubular (i.d. = 10 mm) fixed-bed reactor under atmospheric pressure. A 200 mg of the catalyst was loaded in the reactor. The reaction temperature was monitored by a thermocouple placed in the middle of the catalyst bed. A mixture of 1 vol.% CO and 1 vol.% O₂ balanced by N₂ was introduced as the reactants. The total flow rate was 30 mL min⁻¹, corresponding to a space velocity of 9,000mL g⁻¹ h⁻¹. The CO and CO₂ were analyzed by a gas chromatography (Trace - GC1310) equipped with a FID detector and a TR-WAX column. The gaseous products passed through a methanization converter filled with Raney-Ni catalyst and all the carbon-containing products were converted to methane before they went to the FID detector to ensure a high intensity of signal. Conversion of CO was calculated as follows:

$$\text{CO conversion \%} = \frac{\text{CO}_{\text{in Vol.\%}} - \text{CO}_{\text{out Vol.\%}}}{\text{CO}_{\text{in Vol.\%}}} \times 100$$

where [CO]_{out} and [CO]_{in} are the CO concentrations in the products (vol.%) and feed gas (vol.%), respectively. Carbon balance is near 100 %.

It noted that the analysis procedure of CO concentrations (before and after CO oxidation) was developed from Liu et al.'s work [17].

3. RESULT AND DISCUSSION

3.1. Characterizations of catalysts

3.1.1. Electron microscopy

The electron microscopy image can provide morphology, size, and crystallite property of solid catalyst particle [20]. The TEM images of the CuMnO_x/OMS-2 catalyst are showed in Figure 1. The CuMnO_x/OMS-2 exhibits nanorod-shaped morphologies, with diameters of about 13 nm and lengths of 300–500 nm (Figure 1A). This observation consists with the literatures

result about the related OMS-2 materials [21]. Especially, the Figure 1B (zoomed up from Fig.1A at the red square position) shows the light line on the OMS-2 nanorod surface. It may be the binary metallic oxide nanoparticles of copper and manganese that anchored on the OMS-2 support surface.

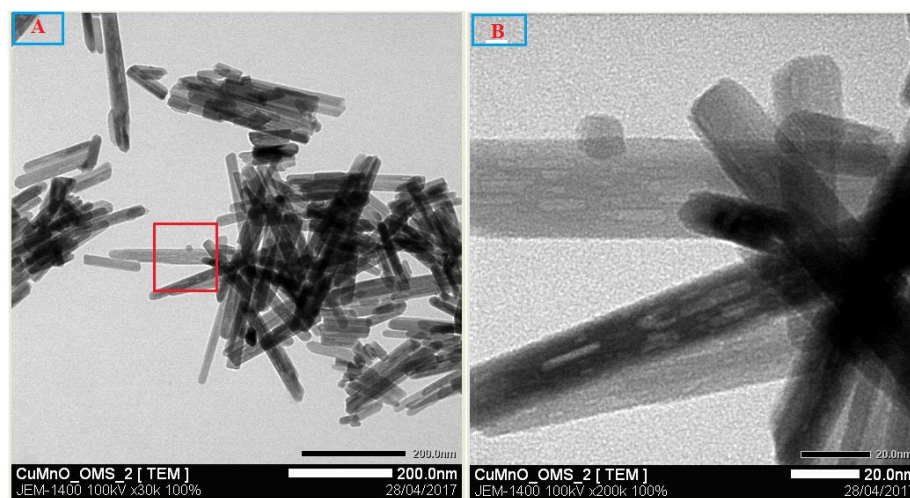


Figure 1. TEM image of $\text{CuMnO}_x/\text{OMS-2}$ material.

3.1.2. XRD, FT-IR, and surface area of catalysts

The XRD patterns of the catalysts are shown in Fig. 2. This Fig. 2 indicates the diffraction peaks at 2θ of 12.6° , 17.9° , 28.7° , 37.5° , 41.9° , 49.9° , and 60.1° which are attributed to the crystalline phase of cryptomelane ($\text{KMn}_8\text{O}_{16}$), indicating that the nanorod OMS-2 material has a cryptomelane-type structure [22]. It consists with the XRD pattern of OMS-2 material in the literatures [21, 22]. However, for XRD pattern of $\text{CuO}/\text{OMS-2}$ catalyst, the diffraction peaks at 2θ of 32.6° , 35.5° , 38.8° are attributed to the crystalline phase of copper oxide [17]. For $\text{CuMnO}_x/\text{OMS-2}$ material, the XRD measurement confirms the presence of crystalline phase of copper oxide due to the detection of one peak at 2θ of 32.6° [17]. Especially, the XRD pattern of $\text{MnO}_x/\text{OMS-2}$ material does not show any differences to that of OMS-2 material, indicating that MnO_x species may be highly dispersed in the sample.

The FT-IR patterns of catalysts are shown in Fig. 3. For $\text{CuO}/\text{OMS-2}$ catalyst, the FT-IR pattern is characterized by oscillations of Cu-O-Cu (410 cm^{-1} , 420 cm^{-1} , and 430 cm^{-1}) and Cu-O (440 cm^{-1}) [23]. These oscillations of Cu-O-Cu (410 cm^{-1} , 420 cm^{-1} , and 430 cm^{-1}) and Cu-O (440 cm^{-1}) [23] are also observed in the FT-IR pattern of $\text{CuMnO}_x/\text{OMS-2}$ material. It consists with the XRD pattern of this material. Additionally, the BET surface area of OMS-2 support is $48.5\text{ m}^2/\text{g}$. However, the BET surface area of other catalysts is lower than that of OMS-2 support (see the Table 1 for detail).

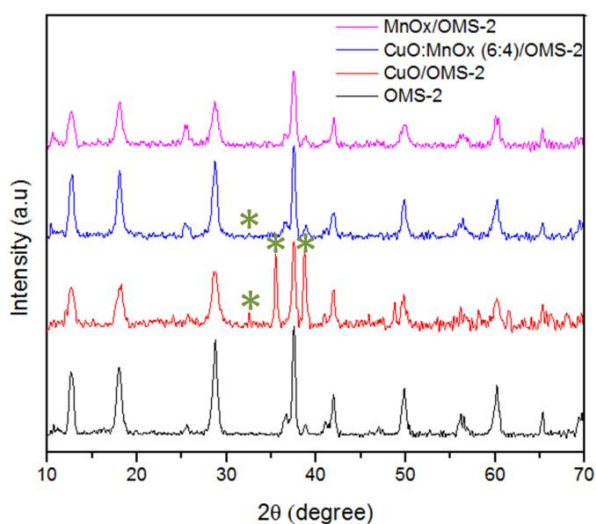


Figure 2. XRD patterns of catalysts (*the peaks are contributed by CuO diffraction).

Table 1. BET surface area, ratio of Cu and Mn of catalysts.

Catalyst	BET surface area (m ² /g)	Cu and Mn concentrations in the fresh solution (g/g)	Ratio of Cu:Mn
OMS-2	48.5	---	---
CuO/OMS-2	41.4	0.11	---
CuMnO/OMS-2	25.9	0.064:0.041	6:4
MnO _x /OMS-2	25.8	0.12	---

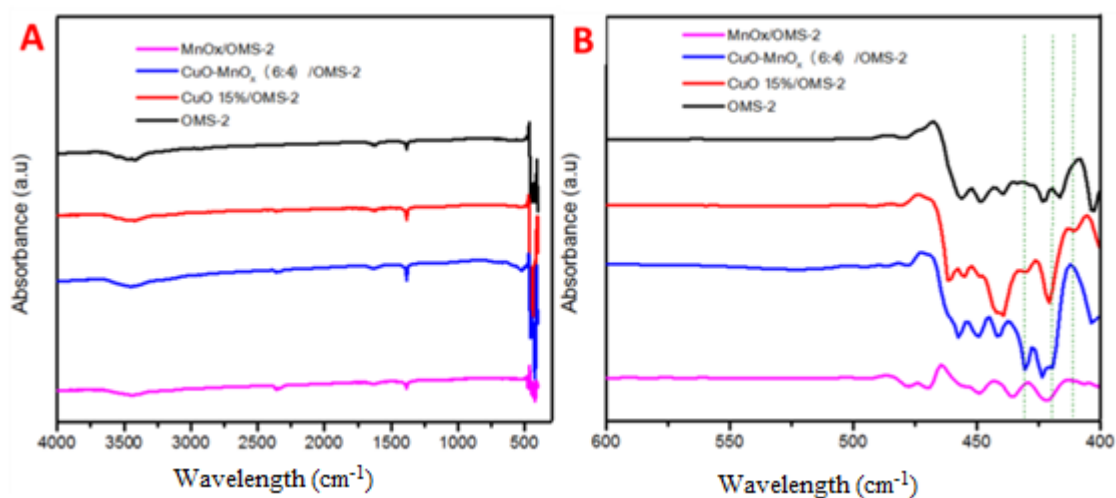


Figure 3. FT-IR patterns of catalysts.

3.1.3. H₂-TPR analysis

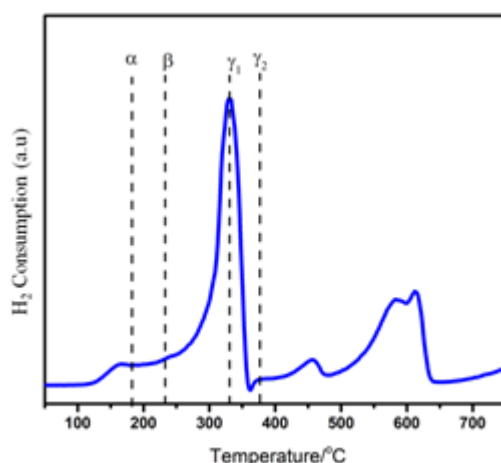


Figure 4. The H₂-TPR profile of CuMnO_x/OMS-2 catalyst.

The redox properties of the catalysts are usually characterized by means of H₂-TPR. Figure 4 shows the H₂-TPR profile of CuMnO_x/OMS-2 catalyst. In comparison to H₂-TPR result of Liu et al.'s [17], two reduction peaks (γ_1 , γ_2) are shifted to lower temperature indicating that the presence of copper promotes the reducibility of manganese oxide through a hydrogen spillover effect. Additionally, the α peak is assigned to the reduction of the CuO_x species that have strong interaction with Mn oxides and the β peak belongs to the reduction of highly dispersed CuO_x species on the catalyst surface which have a weak interaction with the surface Mn oxides or the Cu clusters. Moreover, the appearance of β peak is probably due to a combined reduction of large CuO particles and MnO₂ to Mn₃O₄[24]. Remarkably, the CuMnO_x/OMS-2 catalyst exhibited more excellent reducibility than that of CuO and Mn oxides because of which the collaborative effect between Cu and Mn components as the Cu²⁺-O²⁻ - Mn⁴⁺ structure could enhance the redox potential of metal-oxide species [25]. The reduction temperatures of each peak are summarized in Table 2.

Table 2. The reduction temperature of the peaks in H₂-TPR profile.

Catalysts	α /(°C)	β /(°C)	γ_1 /(°C)	γ_2 /(°C)	Note
CuO/OMS-2	180	275	350	400	Ref. [17]
CuMnO _x /OMS-2	175	245	340	375	This study

3.2. Catalytic performance for CO-oxidation reactions

The CO-oxidation performances of OMS-2, CuO/OMS-2, CuMnO_x/OMS-2, and MnO_x/OMS-2 catalysts are shown in Figure 5. It is noted that the fabricated catalysts were packed and sieved to enhance the stability under the effect of high gas flow rate in the U-reactor. As shown in the Figure 5A, the activated based CuO catalysts on OMS-2 support showed very high activity for CO-oxidation reaction at low temperature. However, the OMS-2 and MnO_x/OMS-2 catalysts showed very low catalytic activities for CO oxidation reaction in the temperature range of this study. The Figure 5A also shows that the full conversion of CO is observed at 55 °C and 65 °C for CuMnO_x/OMS-2 and CuO/OMS-2, respectively. It means that

the CuO based catalyst is the active catalyst for CO oxidation. It consists with the Liu et al. report [17]. The CuO catalysts on OMS-2 support show high catalytic activity for CO oxidation due to the presence of $\text{Cu}^{2+} - \text{O}^{2-} - \text{Mn}^{4+} \leftrightarrow \text{Cu}^{+} - \square - \text{Mn}^{3+} + \text{O}_2$ redox couple [17] in the solid catalyst structure. Especially, $\text{CuMnO}_x/\text{OMS-2}$ catalyst showed higher CO oxidation activity than that of $\text{CuO}/\text{OMS-2}$ catalyst. For example, a lower temperature for full conversion of CO was observed with $\text{CuMnO}_x/\text{OMS-2}$ catalyst. A special rate at $\sim 35^\circ\text{C}$ (room temperature) for CO conversion of $\text{CuMnO}_x/\text{OMS-2}$ catalyst is 1.74 folds better than that of $\text{CuO}/\text{OMS-2}$ catalyst (see the Fig. 5B and Table 3). It could be said that the rate for CO conversion of $\text{CuMnO}_x/\text{OMS-2}$ catalyst is faster than that of $\text{CuO}/\text{OMS-2}$ catalyst. The advanced functionality of binary oxide structure of $\text{CuMnO}_x/\text{OMS-2}$ catalyst is probably due to the higher content of $\text{Cu}^{2+} - \text{O}^{2-} - \text{Mn}^{4+} \leftrightarrow \text{Cu}^{+} - \square - \text{Mn}^{3+} + \text{O}_2$ redox couple.

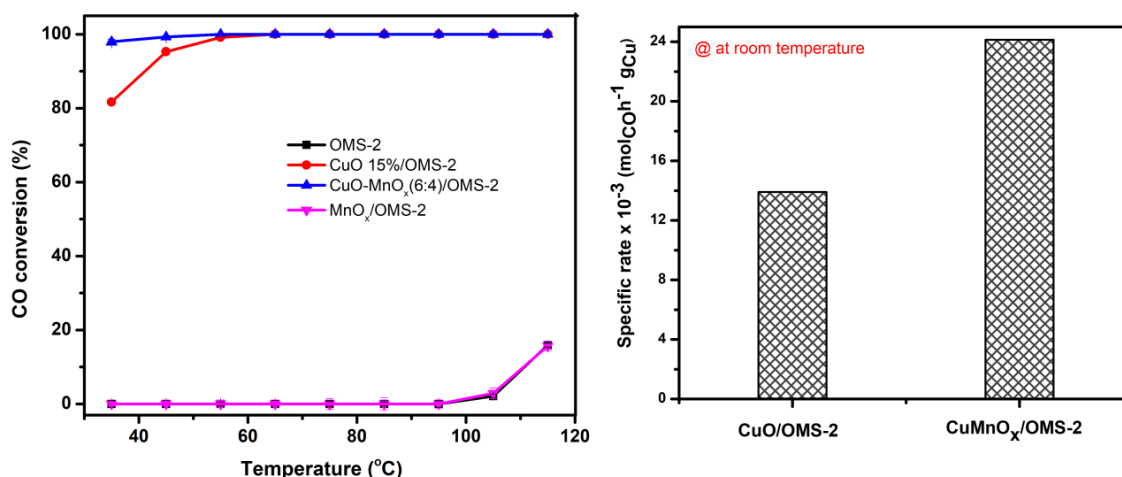


Figure 5. Temperature effects to catalytic activity of CO conversion.

Table 3. Specific rate of catalysis for CO oxidation.

Catalyst	Reaction temperature (°C)	Specific rate (mol _{CO} · h ⁻¹ · g _{Cu} ⁻¹)	Note
CuO/OMS-2	20	11.2×10^{-3}	Ref. [17]
CuO/OMS-2	Room temperature (~35 °C)	13.91×10^{-3}	This study
CuMnO _x /OMS-2	Room temperature (~35 °C)	24.14×10^{-3}	This study

3.3. Catalyst stability for CO-oxidation reactions

Stability tests of $\text{CuO}/\text{OMS-2}$ and CuMnO_x catalysts for CO conversion were performed at room temperature with a constant flow rate of CO. The results are shown in Fig. 6. For $\text{CuO}/\text{OMS-2}$ catalyst, the decreased catalytic activity for CO conversion was observed after 24 hours and no activity for CO conversion was observed after 72 hours. However, for $\text{CuMnO}_x/\text{OMS-2}$ catalyst, the inactivation is observed after 98 hours of stability test. The result showed a better stability of CuMnO_x catalyst for CO oxidation. It is implied that the binary

structure with the advanced composition of manganese may enhance the CuO catalytic activity and stability for CO oxidation.

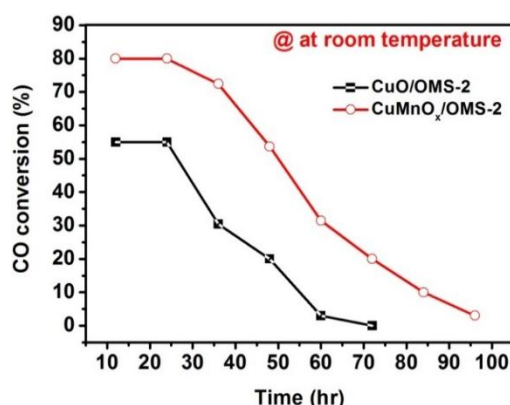


Figure 6. Catalyst stability for CO conversion.

4. CONCLUSIONS

In this study, CuMnO_x/OMS-2 catalysts with various Cu/Mn molar ratio were successfully prepared using the incipient wetness method. A complete conversion of CO at low reaction temperature was observed with the CuMnO_x/OMS-2 catalyst using the 6/4 molar ratio of Cu/Mn. The temperatures at which CO conversion reach 100 % (T_{100}) were as follows: CuMnO_x/OMS-2 (55 °C) < CuO/OMS-2 (65 °C). In addition, the CuMnO_x/OMS-2 showed the catalytic stability better than that of the CuO/OMS-2 catalyst. These results showed that the enhancing catalyst performance of the CuO catalyst in CO oxidation could be assumed by the structure of binary oxide functional with the advanced composition of manganese. This study showed the high application potential of CuMnO_x/OMS-2 material in exhaust treatment for environmental safety.

REFERENCES

1. Zheng X., Zhang X., Fang Z., Wang X., Wang S., Wu S. - Characterization and catalysis studies of CuO/CeO₂ model catalysts, *Catalysis Communications* **7** (9) (2006) 701-704.
2. Zhu H., Qin Z., Shan W., Shen W., Wang J. - Pd/CeO₂-TiO₂ catalyst for CO oxidation at low temperature: a TPR study with H₂ and CO as reducing agents, *Journal of Catalysis* **225** (2) (2004) 267-277.
3. Bollinger M.A., Vannice M.A. - A kinetic and DRIFTS study of low-temperature carbon monoxide oxidation over Au - TiO₂ catalysts, *Applied Catalysis B: Environmental* **8** (4) (1996) 417-443.
4. Wolf A., Schuth F. - A systematic study of the synthesis conditions for the preparation of highly active gold catalysts, *Applied Catalysis A: General* **226** (1) (2002) 1-13.
5. Schryer D. R., Upchurch B. T., Sidney B. D., Brown K. G., Hoflund G. B., Herz R. K. - A proposed mechanism for Pt/SnO_x-catalyzed CO oxidation, *Journal of Catalysis* **130** (1) (1991) 314-317.

6. Luo M.-F., Zhong Y.-J., Yuan X.-X., Zheng X.-M. - TPR and TPD studies of CuO/CeO₂ catalysts for low temperature CO oxidation, *Applied Catalysis A: General* **162** (1) (1997) 121-131.
7. Luo M.-F., Song Y.-P., Lu J.-Q., Wang X.-Y., Pu Z.-Y. - Identification of CuO Species in High Surface Area CuO–CeO₂ Catalysts and Their Catalytic Activities for CO Oxidation, *The Journal of Physical Chemistry C* **111** (34) (2007) 12686-12692.
8. Chen C.-S., You J.-H., Lin J.-H., Chen Y.-Y. - Effect of highly dispersed active sites of Cu/TiO₂ catalyst on CO oxidation, *Catalysis Communications* **9** (14) (2008) 2381-2385.
9. Liu W., Flytzanistephanopoulos M. - Total Oxidation of Carbon Monoxide and Methane over Transition Metal Fluorite Oxide Composite Catalysts: I. Catalyst Composition and Activity, *Journal of Catalysis* **153** (2) (1995) 304-316.
10. Luo M.-F., Ma J.-M., Lu J.-Q., Song Y.-P., Wang Y.-J. - High-surface area CuO–CeO₂ catalysts prepared by a surfactant-templated method for low-temperature CO oxidation, *Journal of Catalysis* **246** (1) (2007) 52-59.
11. Shen Y.F., Zenger R. P., DeGuzman R. N., Suib S. L., McCurdy L., Potter D. I. - Manganese Oxide Octahedral Molecular Sieves: Preparation, Characterization, and Applications. *Science* **260** (5107) (1993) 511-515.
12. Dyer A., Pillinger M., Newton J., Harjula R., Moller T., Amin S. - Sorption Behavior of Radionuclides on Crystalline Synthetic Tunnel Manganese Oxides, *Chemistry of Materials* **12** (12) (2000) 3798-3804.
13. Abecassis-Wolfovich M., Jothiramalingam R., Landau M. V., Herskowitz M., Viswanathan B., Varadarajan T. K. - Cerium incorporated ordered manganese oxide OMS-2 materials: Improved catalysts for wet oxidation of phenol compound, *Applied Catalysis B: Environmental* **59** (1) (2005) 91-98.
14. Gandhe A.R., Rebello J. S., Figueiredo J. L., Fernandes J. B. - Manganese oxide OMS-2 as an effective catalyst for total oxidation of ethyl acetate, *Applied Catalysis B: Environmental* **72** (1) (2007) 129-135.
15. Schurz F., Bauchert J. M., Merker T., Schleid T., Hasse H., Glaser R. - Octahedral molecular sieves of the type K-OMS-2 with different particle sizes and morphologies: Impact on the catalytic properties in the aerobic partial oxidation of benzyl alcohol, *Applied Catalysis A: General* **355** (1) (2009) 42-49.
16. Chen J., Li J., Li H., Huang X., Shen W. - Facile synthesis of Ag–OMS-2 nanorods and their catalytic applications in CO oxidation, *Microporous and Mesoporous Materials* **116** (1) (2008) 586-592.
17. Liu X.-S., Jin Z.-N., Lu J.-Q., Wang X.-X., Luo M.-F. - Highly active CuO/OMS-2 catalysts for low-temperature CO oxidation, *Chemical Engineering Journal* **162** (1) (2010) 151-157.
18. DeGuzman, R.N., Shen Y.-F., Neth E. J., Suib S. L., O'Young C.-L., Levine S. - Synthesis and Characterization of Octahedral Molecular Sieves (OMS-2) Having the Hollandite Structure, *Chemistry of Materials* **6** (6) (1994) 815-821.
19. Singh S., Prasad R. - Physico-chemical analysis and study of different parameters of hopcalite catalyst for CO oxidation at ambient temperature, *Int. J. Sci. Eng. Res.* **7** (4) (2016) 846-855.

20. Nguyen T.-T., Pan C.-J., Liu J.-Y., Chou H.-L., Rick J., Su W.-N. - Functional palladium tetrapod core of heterogeneous palladium–platinum nanodendrites for enhanced oxygen reduction reaction, *Journal of Power Sources* **251** (2014) 393-401.
21. Zhang J., Meng X., Yu C., Chen G., Zhao P.- Heterogeneous Cu/OMS-2 as an efficient catalyst for the synthesis of tetrasubstituted 1,4-enediones and 4H-pyrido[1,2-a]-pyrimidin-4-ones, *RSC Advances* **5** (106) (2015) 87221-87227.
22. Sithambaram S., Nyutu E.K., Suib S.L. - OMS-2 catalyzed oxidation of tetralin: A comparative study of microwave and conventional heating under open vessel conditions, *Applied Catalysis A: General* **348** (2) (2008) 214-220.
23. Arun K., Batra A., Krishna A., Bhat K., Aggarwal M., Francis J. - Surfactant free hydrothermal synthesis of copper oxide nanoparticles. *American Journal of Materials Science* **5** (3A) (2015) 36-38.
24. Luu C.L., Nguyen T., Hoang T. C., Hoang M. N., Ha C. A. - The role of carriers in properties and performance of Pt-CuO nanocatalysts in low temperature oxidation of CO and p-xylene, *Advances in Natural Sciences: Nanoscience and Nanotechnology* **6** (1) (2014) 015011 (9 pages).
25. Liu T., Yao Y., Wei L., Shi Z., Han L., Yuan H.,- Preparation and Evaluation of Copper–Manganese Oxide as a High-Efficiency Catalyst for CO Oxidation and NO Reduction by CO, *The Journal of Physical Chemistry C* **121** (23) (2017) 12757-12770.